Spectroscopy with meV energy resolution

2001 J. Phys.: Condens. Matter 13 7525

(http://iopscience.iop.org/0953-8984/13/34/305)

INSTITUTE OF PHYSICS PUBLISHING JOURNAL OF PHYSICS: CONDENSED MATTER

J. Phys.: Condens. Matter **13** (2001) 7525–7537 PII: S0953-8984(01)24257-X

Spectroscopy with meV energy resolution

Harald Sinn

Advanced Photon Source, Argonne National Laboratory, Argonne, IL 60439, USA

E-mail: sinn@aps.anl.gov

Received 26 April 2001
Published 9 August 2001
Online at stacks.iop.org/JPhysCM/13/7525

Abstract

Inelastic x-ray scattering has become a powerful tool in condensed matter physics in recent years. This is due to the advent of the third-generation synchrotron radiation sources, which provide an intense and collimated x-ray beam, and due to improvements in x-ray optics. This article is an introduction to the basic principles of inelastic x-ray scattering with meV resolution. In particular the geometric and crystal contributions for monochromator and analyser crystals are discussed. Also, an estimation of phonon intensities, obtained with a meV spectrometer, is derived.

1. Introduction

With the advent of third-generation synchrotron radiation sources in the last couple of years, a new method for inelastic spectroscopy has become a powerful tool in condensed matter physics: inelastic scattering of hard x-rays with meV resolution. It resembles inelastic neutron spectroscopy with a triple-axis spectrometer. However, in view of the high energy of the x-rays, a relatively high energy resolution is required in this case. This leads to an extreme backscattering geometry at the monochromator and the analyser crystals.

A spectrometer for inelastic scattering of hard x-rays with meV resolution was proposed first in 1983 by Dorner and Peisl [1]. This instrument is based on two spherically bent crystals in backscattering geometry serving as monochromator and analyser. The realization of such a spectrometer that allows one to measure phonons directly with synchrotron radiation was achieved in 1987 (see Burkel [2] for an overview). The spectrometer was located on a wiggler beamline of the synchrotron radiation source HASYLAB (Hamburger Synchrotron Labor) and operated with an energy resolution of about 10 meV at best. At the European Synchrotron Radiation Facility (ESRF) this kind of spectrometer was further developed on an undulator beamline by Sette *et al* reaching an overall energy resolution between 3 meV and 1.5 meV [3, 4]. Currently, several new inelastic spectrometers are either being built or planned at the third-generation synchrotron sources ESRF in France, the Advanced Photon Source (APS) in the USA [5] and the Super Photon ring 8 GeV (SPring-8) in Japan [6], which will allow energy resolutions between 1 meV and 3 meV and will permit access to this new

kind of spectroscopy to a larger number of users. A recent review covering the development and results from inelastic x-ray scattering can be found in Burkel [7].

The purpose of this article is to give an introduction to this technique and to explain the relevant contributions to the energy resolution. In particular, the backscattering geometry is discussed in detail. In the last section, the intensity for phonon scattering is estimated with respect to dependence on the atomic number. This should help new users of this technique to estimate phonon intensities and the feasibility of an experiment.

2. Scattering cross section

A general inelastic scattering process is sketched in figure 1: an x-ray or neutron beam with a certain monochromatic energy E_i and wave vector $\vec{k}_i$ is hitting the sample. Inside the sample an inelastic process is excited with an energy $E = \hbar\omega$ (in the following it is just referred to as ω) and momentum transfer $\hbar\vec{Q}$.

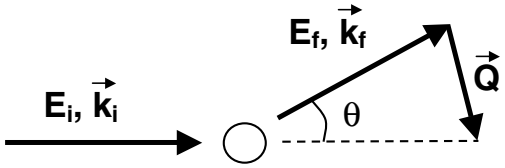

Figure 1. A schematic diagram of an inelastic scattering process.

The scattered beam with energy E_f and wave vector $\vec{k}_f$ is shifted by this energy ω and is deflected by the angle θ. From the conservation of energy and momentum it follows that

$$\omega = E_i - E_f \tag{1}$$

and

$$\vec{Q} = \vec{k}_i - \vec{k}_f. \tag{2}$$

If now the energy shift of the scattered radiation is analysed at a certain scattering angle, one can measure the energies of excitations related to a certain length scale. The cross section for non-resonant inelastic x-ray scattering is (see e.g. [8])

$$\frac{\mathrm{d}^2\sigma}{\mathrm{d}\Omega\,\mathrm{d}\omega}(\vec{Q},\omega) = r_e^2(\vec{e}_i\cdot\vec{e}_f)^2\frac{E_f}{E_i}N\left[f^2(Q)S_{\mathrm{ion}}^{\mathrm{coh}}(\vec{Q},\omega) + zS_{\mathrm{val}}^{\mathrm{inc}}(\vec{Q},\omega) + (Z-z)S_{\mathrm{ion}}^{\mathrm{inc}}(\vec{Q},\omega)\right] \tag{3}$$

with r_e the classical electron radius, N the number of atoms in the beam and $\vec{e}_i$, $\vec{e}_f$ the polarization vectors of the incoming and scattered radiation. $S_{\mathrm{ion}}^{\mathrm{coh}}(\vec{Q},\omega)$ is the coherent dynamic structure factor for the ions, which is identical to the coherent dynamic structure factor that can be observed with inelastic neutron scattering. Within the adiabatic approximation it is assumed that the electrons move instantaneously with the whole atom, and therefore the coherent correlation functions observed from the nuclei and from the electron clouds have the same energy dependence. For the valence electrons, however, the atomic form factor might be different from the atomic form factor for the free atom, usually found in the standard literature. Therefore, the form factor is split up into a part for the core electrons, $f_{\mathrm{ion}}(Q)$, and a part for the valence electrons $f_{\mathrm{val}}(Q)$ [9]:

$$f(Q) = f_{\mathrm{ion}}(Q) + f_{\mathrm{val}}(Q). \tag{4}$$

The part for the valence electrons is related to the valence electron density distribution between the ions, information that cannot be extracted from inelastic neutron scattering. The determination of the form factor at low Q can yield in principle a direct insight into properties like the electron gas compressibility [10] or the pseudopotential between ions and electrons in a metal. However, this requires a precise determination of phonon intensities [11].

The other parts of the cross section are incoherent scattering from valence electrons, $zS^{\mathrm{inc}}_{\mathrm{val}}(\vec{Q},\omega)$, with z being the number of valence electrons, and incoherent scattering from core electrons, $(Z-z)S^{\mathrm{inc}}_{\mathrm{ion}}(\vec{Q},\omega)$, with Z being the total number of electrons. These excitations are typically at much higher energies than the coherent phononic excitations. In a measurement with meV resolution, the incoherent scattering contributions are less intense and usually invisible, unless one tunes the energy transfer to several eV. Therefore the relevant part for measurements with meV resolution is the coherent structure factor $S^{\mathrm{coh}}_{\mathrm{ion}}(\vec{Q},\omega)$.

There are several practical limitations on the determination of $S^{\mathrm{coh}}_{\mathrm{ion}}(\vec{Q},\omega)$ that occur in neutron scattering that are absent in inelastic x-ray scattering. First, neutrons are classical particles, with a certain velocity. If the phase velocity of the excitation in the sample is higher than the flight velocity of the neutrons, these excitations cannot be observed in the scattering process due to kinematical restrictions. Second, certain isotopes like ^{3}He or hydrogen are extremely difficult to investigate with neutrons, because of a high absorption or a large incoherent cross section. And finally, neutron scattering requires large samples because of the large beam size. The undulator beam of a third-generation synchrotron source can be focused with almost no losses to a few micrometres in size.

In fact, inelastic x-ray scattering and inelastic neutron scattering can be regarded as complementary techniques: if an energy resolution of less than 1 meV is required and a large sample can be prepared, inelastic neutron scattering will be in general favourable. For small sample volumes and if excitations are at relatively high energies, inelastic x-ray scattering will be the more suitable technique. The combination of these two techniques bears also the possibility of looking at the dynamics of specific atoms in, e.g., alloys, since the element-specific cross sections are entirely different for the two techniques.

3. Basic relations

The required relative energy resolution is about

$$\frac{\delta E}{E_i} \approx \frac{1\ \mathrm{meV}}{20\ \mathrm{keV}} = 5\times 10^{-8}. \tag{5}$$

Because the energy transfer ω is small compared to E_i, the magnitude k_i of the x-ray wave vector does not change significantly during the scattering process. According to figure 1, the magnitude of the momentum transfer in equation (2) can therefore be written as

$$Q = 2k_i \sin\theta/2 = \frac{2E_i}{\hbar c}\sin\theta/2 \tag{6}$$

$$Q\ (\mathrm{\AA}^{-1}) = 1.013E_i\ (\mathrm{keV})\sin\theta/2. \tag{7}$$

Consequently, the momentum transfer can be adjusted by changing the scattering angle at the sample, independently of the energy transfer. This is very useful, because the entire $(\vec{Q},\omega)$-space is accessible with practically the same resolution in momentum and energy. The momentum resolution can be adjusted with slits defining the divergences of the incoming and the scattered radiation.

The energy resolution depends on different quantities, in particular on the quality of the monochromator and analyser crystals (crystal contributions) and on Bragg angle variation

at these crystals, which leads also to a broadening of the resolution function (geometry contributions). Accordingly, the resolution function, $R(\omega)$, can be written as the convolution of four distributions:

$$R(\omega) = R^{\text{mono}}_{\text{crystal}}(\omega) \otimes R^{\text{mono}}_{\text{geom}}(\omega) \otimes R^{\text{ana}}_{\text{crystal}}(\omega) \otimes R^{\text{ana}}_{\text{geom}}(\omega). \tag{8}$$

In the following, the crystal contribution and the geometry contribution will be discussed in more detail.

3.1. Crystal contribution for a perfect crystal

The crystal contribution is the energy distribution of a parallel, white x-ray beam reflected by a flat crystal. If the crystal is strained or not perfect, a distribution of lattice spacings will lead to a distribution of reflected energies. Since the desired energy resolution is in the range of $\delta E/E \approx 10^{-8}$, the relative lattice spacing variation should be of that order or smaller. This condition can be met by today's available float-zone silicon crystals, if the mounting is achieved free of strain and if any stress from cutting and polishing is removed by subsequent etching procedures.

But even for a perfect crystal, the reflected energy has a width larger than zero, because the x-ray beam is reflected only by a more or less thin layer at the surface of the crystal (extinction length τ_{ext}). This leads to an uncertainty in the reflected energy or, more precisely, to the energy distribution, which corresponds to $R^{\text{mono}}_{\text{crystal}}(\omega)$ and $R^{\text{ana}}_{\text{crystal}}(\omega)$ in equation (8). This distribution can be calculated by the dynamic theory of crystal reflection and is called the Darwin curve.

The exact dynamic theory for perfect crystals can be found in standard textbooks on x-ray scattering [12]. For the width of the Darwin curve, δE, depending on energy or wavelength λ, one finds

$$\frac{\delta E_{\text{crystal}}}{E} = \frac{\delta\lambda}{\lambda} = \frac{r_e \lambda^2 F(\vec{G})}{\pi V \sin^2\theta_B} \propto \frac{1}{\tau_{\text{ext}}}. \tag{9}$$

One important result is that the energy width of the reflected intensity does not change much with the Bragg angle θ_B close to backscattering. This is why the resolution function can be split up conveniently into geometric and crystal contributions in equation (8). The structure factor $F(\vec{G})$ is the sum of the coherent scattering in the direction of the reciprocal-lattice vector $\vec{G}$ from all atoms in the unit cell of volume V. It includes the Debye–Waller factor and the atomic form factor.

Another consequence of equation (9) is that the energy width becomes drastically smaller at higher energies or smaller wavelength. The smaller δE, the larger the extinction length τ_{ext}. In equation (9) the photoelectric absorption, which sets an upper bound to the extinction length, was neglected. In table 1 these widths as calculated from the full dynamic theory for silicon are given[1]. For high-order reflections, the energy resolution becomes better, but also the reflectivity drops due to a more unfavourable ratio of extinction to absorption length at higher energies.

Equation (9) is only true as long as the so-called two-beam condition is fulfilled, which means that there is one incoming beam and one reflected beam. For certain crystal orientations, however, more than one Bragg reflection might be excited, which is then called a multiple-beam case. In this situation, the intensity of the desired reflection can be considerably reduced and also side maxima in the Darwin curve can occur.

A detailed study of this phenomenon was done by Sutter and co-workers [13]. It turns out that in a silicon crystal practically every reflection close to perfect backscattering geometry

[1] Results are calculated for a temperature of 300 K and a thick crystal with the program *reflex* written by Y Shvydko.

Table 1. Crystal contributions for different silicon reflections. The reflections are higher orders of the (1, 1, 1) and the (3, 1, 0) reflections, currently used at the existing spectrometers.

Reflection	E (keV)	τ_{ext} (μm)	τ_{abs} (μm)	$\delta E_{\text{crystal}}$ (meV)	Reflectivity (%)
(7, 7, 7)	13.839	40	300	5.13	81
(12, 4, 0)	14.438	30	380	6.21	87
(8, 8, 8)	15.816	50	500	4.42	85
(9, 9, 9)	17.793	100	700	1.99	76
(18, 6, 0)	21.657	200	1220	1.23	78
(11, 11, 11)	21.747	280	1240	0.85	70
(12, 12, 12)	23.724	270	1590	0.79	75
(13, 13, 13)	25.701	600	1990	0.37	61
(24, 8, 0)	28.876	840	2730	0.255	61
(15, 15, 15)	29.655	1400	2930	0.153	46

is a multiple-beam case, typically with twenty or more beams involved. However, for Bragg angles a few millidegrees away from backscattering, multiple-beam effects can be in principle avoided by choosing a certain crystal orientation. Another way to get around this problem is to use crystals other than silicon, which have a non-cubic crystal symmetry. Then, however, it becomes difficult to obtain crystals of a high enough quality. The best resolution obtained so far from a non-silicon crystal is 2.5 meV from a sapphire crystal at 21.5 keV in exact backscattering geometry [14].

In the following we assume that multiple-beam situations can be avoided in one way or the other and that therefore there is no significant dependence of the crystal contribution on small variations of the Bragg angle.

3.2. Geometry contribution for a flat crystal

A distribution of reflected wavelengths arises from the fact that the incident angle for a divergent beam varies over the crystal surface. From a differentiation of the Bragg law one can easily derive

$$\frac{\delta E_{\text{geom}}}{E} = \text{cotan}(\theta_B)\,\delta\theta_B = \tan(\epsilon)\,\delta\epsilon \approx \epsilon\,\delta\epsilon \tag{10}$$

with $\epsilon = \pi/2 - \theta_B$. Close to backscattering, $\tan(\epsilon)$ can be replaced by ϵ. In contrast to the crystal contribution, the geometry contribution depends strongly on the Bragg angle. As a consequence, a geometry close to perfect backscattering geometry is required for a meV spectrometer at the monochromator and analyser crystals. However, even in perfect backscattering geometry, the energy width in equation (10) does not go to zero, as can be seen in figure 2(a), if the angular divergence of the beam $\delta\epsilon_{\text{beam}}$ is finite. On the surface of the crystal, the Bragg angle is constant on circles (dotted lines in figure 2) around the backscattering point, where $\epsilon = 0$. In this case, although the crystal is aligned to perfect backscattering, the average Bragg angle is about $\frac{1}{4}\,\delta\epsilon_{\text{beam}}$. The width of the Bragg angle distribution in equation (10) is about $\delta\epsilon = \frac{1}{2}\,\delta\epsilon_{\text{beam}}$. Therefore,

$$\frac{\delta E_{\text{geom}}}{E} \approx \tfrac{1}{8}(\delta\epsilon_{\text{beam}})^2. \tag{11}$$

In a real experiment this geometry can be achieved at the analyser with a semitransparent detector with a sufficient time resolution (e.g., as in [14]). However, because of the limited efficiency of this set-up, a geometry slightly off exact backscattering is preferred for a spectrometer (see figure 2(b)). For an estimation of the width of the Bragg angle distribution,

one can approximate $\delta\epsilon \approx \delta\epsilon_{\mathrm{beam}}$ in the scattering plane of the back-reflection and $\epsilon \approx \langle\epsilon\rangle$, the Bragg angle in the centre of the beam cone.

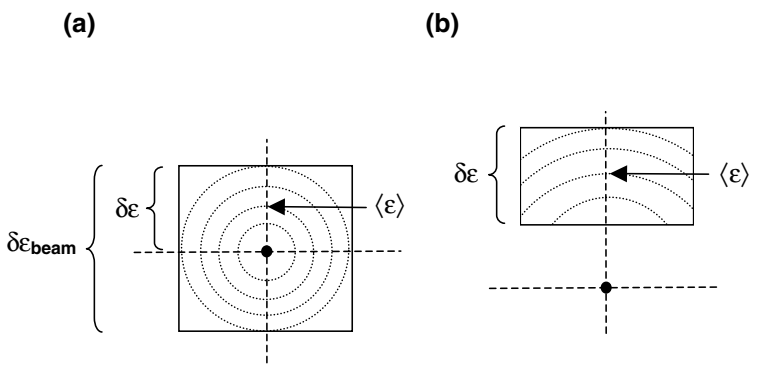

Figure 2. Distribution of scattering angles in perfect backscattering geometry (a) and close to perfect backscattering (b). The rectangle is an area on the crystal that is illuminated by the beam. The black point is the backscattering point. The Bragg angle is constant on the dotted lines.

For a detailed calculation of the shape of the resolution function, one has to integrate over the distribution of Bragg angles on the illuminated two-dimensional crystal surface [15].

3.3. Geometry contribution for a curved crystal

In inelastic x-ray scattering, crystals are spherically bent for two reasons: first, to focus the intensity that is collected in a larger solid angle to a small detector and, second, to maintain the same or similar Bragg angle all over the crystal. The focusing behaviour is the same as for a mirror with optical light and can be described by the lens equation

$$\frac{1}{L} + \frac{1}{l} = \frac{2}{R} \tag{12}$$

where R is the bending radius of the mirror, L is the distance from source to mirror and l is the distance from mirror to focus. In the case of perfect backscattering, the source and image are both in the centre of the sphere and the Bragg angle is constant all over the crystal; that is, $\epsilon = 0$.

For $L \neq l$ and for a tangential distance $d \ll R$ between the sample and the detector, the Bragg angle at a small distance s from the backscattering point is (see figure 3)

$$2\epsilon = \frac{s - d/2}{l} - \frac{s + d/2}{L}. \tag{13}$$

To calculate the Bragg angle distribution, one has again to consider the two-dimensional crystal surface. Here, we estimate this contribution for a situation close to backscattering by differentiating equation (13):

$$2\,\delta\epsilon = \delta s\left(\frac{1}{l} - \frac{1}{L}\right). \tag{14}$$

The distance $\delta s \equiv D$ can be understood as the slit opening in front of the crystal. The ratio L/l is also called the demagnification ratio. Equation (14) can therefore be rewritten as

$$\delta\epsilon_{\mathrm{demag}} = \frac{D}{2L}\left(\frac{L}{l} - 1\right). \tag{15}$$

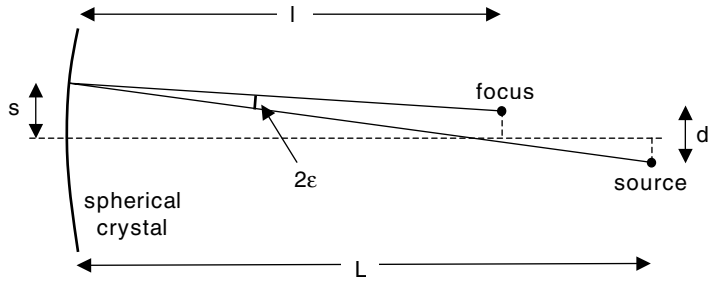

Figure 3. The geometry contribution for a curved crystal. One particular beam is shown, which is reflected from the source to the focus.

The part of the energy resolution function arising from equation (15) is called the demagnification contribution. By choosing the demagnification ratio close to one, it is possible to reduce the geometrical contribution to a fraction of an meV, even over a large solid angle. At the same time the radiation is focused to a small area, which makes it convenient to collect it with a solid-state detector. With a small detector or a slit in front of the detector, a bad focusing part of the analyser will not hit the detector and degrade the energy resolution. Therefore, focusing errors of the analyser will only affect the efficiency of the analyser but not the energy resolution.

4. The monochromator

An undulator beam of a synchrotron source has typically a vertical divergence of about 20 μrad or less. According to equation (10) one can achieve a geometrical contribution from a flat crystal of $\delta E/E \leqslant 5 \times 10^{-8}$ with $\epsilon_{\mathrm{mono}} \leqslant 2.5$ mrad. The use of just one crystal in backscattering geometry is the conceptually easiest design for a monochromator and has the advantage of a high efficiency [16]. This has two consequences. First, the monochromator has to be far away from the sample to have a sufficient beam separation at the sample position. A separation of 10 cm requires in our example a distance of about 20 metres. Additional optical elements like mirrors or other crystals can be brought into the beam path to increase this offset.

The second consequence is that a tuning of the energy cannot be done by a variation of the Bragg angle. Changing the Bragg angle to larger ϵ would increase the geometry contribution and a change to smaller ϵ is not possible because of the space limitations.

Therefore, it is more convenient to tune the energy by changing the lattice constant of the crystal. From the definition of the thermal expansion and from Bragg's law it follows that

$$\frac{\omega}{E_i} = \alpha \, \Delta T \tag{16}$$

where α is the thermal expansion coefficient (2.56×10^{-6} for silicon at room temperature [17]). A temperature difference of $\Delta T = 1$ K between monochromator and analyser leads to an energy shift of 51 meV for silicon at 20 keV. An energy scan can be done conveniently by scanning the temperature over a few K.

Another way to build a tunable monochromator is to reduce the divergence of the undulator beam by using asymmetrically cut crystals. If the divergence is reduced to under 1 μrad, the Bragg angle can be as large as 50 mrad before the geometry contribution becomes dominant. This relaxes the backscattering geometry with the result that even a backscattering channel-cut crystal can be used. Energy tuning can be achieved by rotating the channel cut on a μrad scale,

without noticeable beam motion. However, because of equation (16), the monochromator and the analyser have to be kept in a stable temperature environment.

This idea was realized by Toellner [18] and allows a tunability range up to ±100 eV at an energy resolution of 1.4 meV. Because the beam leaves the monochromator in a forward direction, it is also called an in-line monochromator. In contrast to the case for a single-crystal backscattering monochromator, it is relatively easy to integrate it into a standard beamline design (see also figure 4).

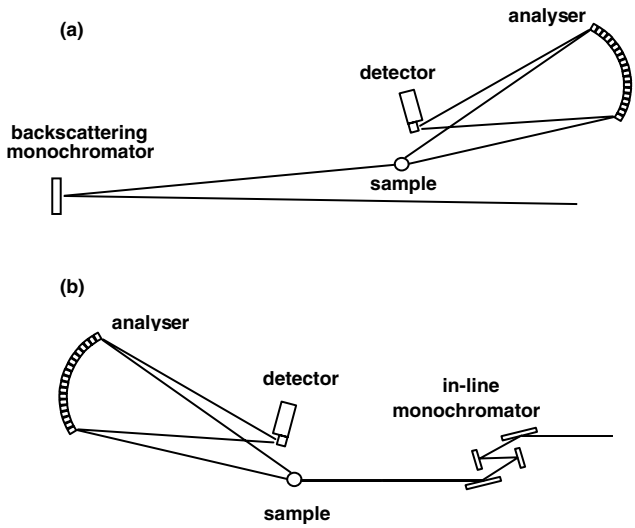

Figure 4. The design of a meV spectrometer with a backscattering monochromator (a) and with an in-line monochromator (b).

5. The analyser

At the analyser, the divergence of the beam coming from the sample is larger than in the case of the monochromator. Typically one tries to collect the radiation in a range of $1^\circ \times 1^\circ$. As described above, this can be done by spherically bent crystals in backscattering geometry. However, to avoid bending stress, the analyser has to be cross grooved at the reflecting surface. Therefore the analyser consists of many small flat crystals that are glued to a sphere (see e.g. [4]). Two geometry contributions have to be considered: the demagnification contribution and the flat-crystal contribution for an individual crystal pixel. In the following we derive all the settings for the analyser depending on the energy resolution and the available pixel size at the analyser. The beam divergence at a pixel with size p in a distance L from a point source is

$$\delta\epsilon_{\text{pixel}} = \frac{p}{L}. \tag{17}$$

In an experiment it is often crucial to have some amount of space around the sample to accommodate certain sample environments like a furnace or a cryostat. On the other hand, the x-ray detector has to be close to the sample to keep the demagnification contribution small. If the demagnification contribution (15) is chosen to be of the same order or smaller than the pixel size contribution (17),

$$\frac{D}{2L}\left(\frac{L}{l} - 1\right) \leqslant \frac{p}{L}. \tag{18}$$

With $\Delta L = L - l$ it follows that

$$\Delta L \leqslant p\frac{2l}{D} \approx 115p \tag{19}$$

if the opening angle of the analyser is $\arctan(D/l) \approx 1^\circ$. If the pixel contribution and the demagnification contribution are equal, the width of the convoluted Bragg angle distributions can be approximated with

$$\delta\epsilon_{\text{ana}} = ((\delta\epsilon_{\text{pixel}})^2 + (\delta\epsilon_{\text{demag}})^2)^{1/2} = \sqrt{2}\epsilon_{\text{pixel}} = \sqrt{2}\frac{p}{L}. \tag{20}$$

A lower limit for the Bragg angle ϵ_{ana} comes from the requirement that the source and the image have to be separated at the location of the detector. Since the image is at least twice the pixel size, it follows that

$$\epsilon_{\text{ana}} > \frac{p}{L}. \tag{21}$$

With a semiconductor detector optimized to this extreme backscattering geometry, it is possible to get close to this value:

$$\epsilon_{\text{ana}} \approx \frac{3p}{2L}. \tag{22}$$

Inserting equations (20) and (22) into equation (10) and solving for L yields

$$L = p\left(\frac{3E}{\sqrt{2}\delta E^{\text{ana}}_{\text{geom}}}\right)^{1/2}. \tag{23}$$

All dimensions for the analyser settings are defined by equations (22), (23) and (19) and scale with the dimension of the pixel size. The pixel size that can be achieved with high-speed diamond saws is limited by the minimum size of a blade that can cut a couple of mm deep into silicon. Currently, with a width of the cut after etching of 0.1 mm to 0.2 mm, a minimum pixel size of about 1 mm seems acceptable, with 20%–40% of the area being lost. Reducing the pixel size in order to shorten the analyser arm would not only affect the analyser efficiency, but according to equation (19) it would also reduce the available space at the sample. Examples of analyser settings for different energy resolutions are discussed in the next section.

6. Design of a meV spectrometer

Putting together the information from the previous section, it is straightforward to understand the basic design parameters of a specific spectrometer. The quantity to start with is the desired energy resolution of the whole spectrometer. Since there are crystal contributions and geometry contributions for both monochromator and analyser, it is a good match if all contributions in equation (8) are of the same width. That means that each individual contribution has to be about half of the desired overall energy resolution. The crystal contribution defines the silicon reflection and the energy of the x-rays that can be used. The setting of the monochromator and of the analyser can be calculated such that this crystal contribution is matched. An overview of settings for different energy resolutions is given in table 2. Notice that these parameters are calculated from the previous approximations. In a real spectrometer, the values for the overall energy resolution are usually about 10%–20% smaller. The reason is the neglect of the shape of the individual parts of the resolution function in the calculation.

An energy resolution of 10 meV can be achieved with an analyser arm of 2 to 3 m, which can conveniently be operated in the vertical scattering geometry. For a better resolution, a longer analyser set-up is required, which is easier to achieve in the horizontal scattering geometry.

Table 2. Settings for the analyser for different energy resolutions. The total energy resolution is here twice the value of the geometrical contribution of the analyser.

δE_{total} (meV)	δE_{geom} (meV)	Reflection	E (keV)	θ_{Bragg} (deg)	L (m)
12.42	6.21	(12, 4, 0)	14.438	89.95	2.22
10.26	5.13	(7, 7, 7)	13.839	89.96	2.39
8.84	4.42	(8, 8, 8)	15.816	89.97	2.76
3.98	1.99	(9, 9, 9)	17.793	89.976	4.35
2.46	1.23	(18, 6, 0)	21.657	89.983	6.11
1.70	0.85	(11, 11, 11)	21.747	89.986	7.36
1.58	0.79	(12, 12, 12)	23.724	89.989	7.98
0.74	0.37	(13, 13, 13)	25.701	89.991	12.1
0.51	0.255	(24, 8, 0)	28.876	89.993	15.5
0.30	0.153	(15, 15, 15)	29.655	89.995	20.2

The drawback of the horizontal scattering geometry is that, for higher scattering angles, the intensity is decreasing, due to the horizontal polarization of the synchrotron radiation and the polarization-dependent term in equation (3).

For very good energy resolutions of less than 1 meV, the length of the analyser arm exceeds 10 metres, so it becomes difficult to build and to integrate in a beamline design. Also, the Bragg angles become very close to backscattering, which will lead to more problems with the multiple-beam excitations. However, the most important limitation that currently restricts the energy resolution to above 1 meV is the available flux at a third-generation synchrotron source. A possibility to improve the flux situation is the installation of multiple analysers, which was first done at the spectrometers at the ESRF. This requires even more instrumentation effort on the analyser side, but multiplies the amount of data that can be taken per time unit. An estimation of the flux will be given in the next section.

In figure 4(a) the design is sketched for an instrument with a backscattering monochromator, which is used at two instruments at the ESRF (ID16 and ID28) and planned for a spectrometer at SPring-8 (BL35XU). Figure 4(b) shows the set-up with an in-line monochromator, currently used at the APS spectrometer (SRI-3ID-C).

7. Phonon intensities

The intensity from phonon scattering can be estimated for small values of Q. We start from equation (3) and omit the terms for electronic scattering. Also, we can assume that $E_f/E_i \approx 1$ and for small scattering angles $\vec{e}_i \parallel \vec{e}_f$, thus

$$\frac{\mathrm{d}^2\sigma}{\mathrm{d}\Omega\,\mathrm{d}\omega}(\vec{Q},\omega) = r_e^2 N f(Q)^2 S_{\text{ion}}^{\text{coh}}(\vec{Q},\omega). \tag{24}$$

For $S(\vec{Q},\omega)$ we apply the one-phonon cross section for a crystal with one atom per unit cell [19]:

$$S(\vec{Q},\omega) = \mathrm{e}^{-2W(\vec{Q})}\frac{\hbar}{2M\omega_0}|\vec{Q}\cdot\vec{e}_{\vec{Q}}|^2\,[(n+1)\delta(\omega-\omega_0)+n\delta(\omega+\omega_0)] \tag{25}$$

where ω_0 is the phonon frequency. At small Q the Debye–Waller factor $\mathrm{e}^{-2W(\vec{Q})}$ becomes one and the eigenvector $\vec{e}_{\vec{Q}}$ for the longitudinal acoustic phonons becomes parallel to $\vec{Q}$. The occupation number n of an acoustic phonon can be approximated for small Q and ω_0 by

$$n = \frac{1}{\mathrm{e}^{(\hbar\omega_0/[k_BT])}-1} \approx \frac{k_BT}{\hbar\omega_0} \gg 1. \tag{26}$$

Therefore the magnitudes of the phonon creation and annihilation parts become equal:

$$S(Q \to 0, \omega) = \frac{Q^2 k_B T}{2M\omega_0^2} \left[\delta(\omega - \omega_0) + \delta(\omega + \omega_0)\right]. \tag{27}$$

Integration over ω yields

$$S(Q \to 0) = \frac{Q^2 k_B T}{M\omega_0^2}. \tag{28}$$

For acoustic phonons, the frequency ω_0 is proportional to the sound velocity v in the sample:

$$\omega_0 = vQ \tag{29}$$

and (28) becomes

$$S(Q \to 0) = \frac{k_B T}{Mv^2}. \tag{30}$$

A similar relation can also be derived for liquids and is known as the compressibility limit of $S(Q \to 0)$ (see e.g. [20]). Inserting relation (30) into (24) and integrating (24) over ω yields

$$\frac{\mathrm{d}\sigma}{\mathrm{d}\Omega}(Q \to 0) = r_e^2 N Z^2 \frac{k_B T}{Mv^2} \tag{31}$$

with $f(Q \to 0) = Z$. Now, we consider an experiment in transmission geometry with a sample thickness $l = l_{\mathrm{abs}}$, the photoelectric absorption length in the sample for the particular energy. At this thickness, the transmitted beam is attenuated to $1/\mathrm{e}$ and a maximum count rate from the sample can be expected. The number of atoms in the sample is $N = A\rho l_{\mathrm{abs}}$, with A being the geometrical cross section of the sample in beam direction and ρ the number density;

$$\frac{\mathrm{d}\sigma}{\mathrm{d}\Omega}(Q \to 0) = r_e^2 \frac{1}{\mathrm{e}} l_{\mathrm{abs}} A\rho Z^2 \frac{k_B T}{Mv^2}. \tag{32}$$

With the definition

$$\frac{\mathrm{d}\sigma}{\mathrm{d}\Omega}(Q) = \frac{I}{I_0}\frac{A}{\Omega} \tag{33}$$

of the scattering cross section, one obtains

$$\frac{I}{I_0} = r_e^2 \Omega \frac{1}{\mathrm{e}} l_{\mathrm{abs}} \rho Z^2 \frac{k_B T}{Mv^2}. \tag{34}$$

I denotes the scattered intensity in the solid angle Ω, and I_0 is the incident intensity hitting the sample. In order to compare the scattered intensities for different incident energies, the solid angle Ω is now chosen in such a way that the momentum resolution remains constant. For small angles θ the sine function in equation (6) can be approximated to be linear. Therefore,

$$\Omega = (\delta\theta)^2 \approx \left(\frac{\delta Q}{k_i}\right)^2 = \left(\frac{\hbar c\, \delta Q}{E_i}\right)^2. \tag{35}$$

The integrated intensity discussed above includes the Stokes and the anti-Stokes line of an acoustic phonon. Since we are interested in the intensity of just one phonon, we take half of the value in equation (34) and combine it with equation (35):

$$\frac{I}{I_0} = \frac{r_e^2 \hbar^2 c^2 (\delta Q)^2}{2\mathrm{e} E_i^2} Z^2 \rho l_{\mathrm{abs}} \frac{k_B T}{Mv^2}. \tag{36}$$

Now we can estimate the scattered intensity from equation (36) for different chemical elements. In figure 5 this is done for two different x-ray energies at 21.657 keV and at 14.438 keV for a momentum resolution of $\delta Q = 1\ \mathrm{nm}^{-1}$. The scattered intensities are in the region of 10^{-8} of

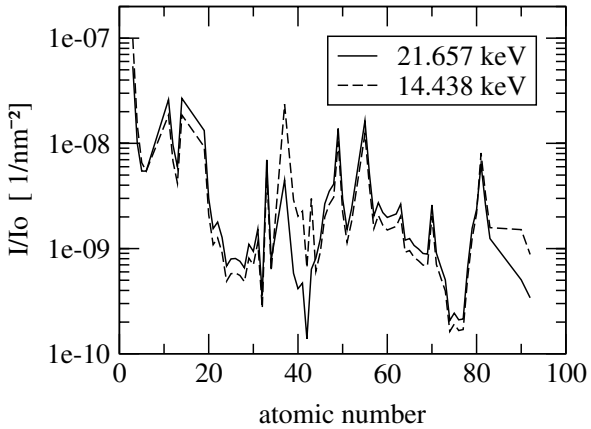

Figure 5. Expected phonon intensities for different elements in forward scattering, normalized to the flux on the sample and 1 nm^{-2} momentum resolution .

the incoming intensity but can vary by about a factor of ten around that value, depending on the location of the absorption edges and the sound velocity of a particular chemical element.

From a state-of-the-art synchrotron source, the theoretical available flux is of the order of 10^{10} s^{-1} meV^{-1}. Taking into account losses in the monochromatization and at the analyser and losses due to a non-ideal sample geometry, the typical count rates in an inelastic scattering experiment are often of the order of 1 count s^{-1} or below. A lower limit for the count rate is given by the electronic noise level of the x-ray detector, which is about 5×10^{-3} counts s^{-1}.

One has to keep in mind that these numbers are calculated for phonons at small momentum transfers. In single crystals, phonons can be measured also in higher Brillouin zones, which can yield considerably higher count rates, because of the Q^2-dependence in the phonon cross section in equation (25). In liquids and amorphous materials, however, phonons can be observed usually only at low Q; therefore most of these experiments are flux limited. One further complication in disordered materials is that the tail of a fairly strong elastic line is superimposed on the phonon intensity.

8. Conclusions

The strength of inelastic x-ray scattering lies in its utility in investigating small samples and liquid or amorphous samples in the low-Q region. To obtain energy resolutions in the range of 1 meV to 3 meV, large instruments with optimized crystal optics are required. Most experiments today with inelastic x-ray scattering are flux limited. This requires careful planning of the experiment and counting times similar to those in neutron spectroscopy. Also it requires the strongest available sources for hard x-rays, currently the ESRF, the APS or SPring-8. Therefore, the amount of available time for experiments is restricted, but with the installation of new instruments in the future this technique will become more accessible to users.

Acknowledgments

This work was supported by the US DOE BES Materials Sciences contract No W-31-109-ENG-38 and the *Euro Summer School 2000: New Materials and their Dynamics Advances through Synchrotron Radiation* organized by Professor Burkel in Rostock.

References

[1] Dorner B and Peisl H 1983 *Nucl. Instrum. Methods* **208** 587
[2] Burkel E 1991 *Inelastic Scattering of X-rays with Very High Energy Resolution* (Berlin: Springer)
[3] Sette F, Ruocco G, Krisch M, Bergmann U, Masciovecchio C, Mazzacurati V, Signorelli G and Verbeni R 1995 *Phys. Rev. Lett.* **75** 850
[4] Masciovecchio C *et al* 1996 *Nucl. Instrum. Methods* B **111** 181
[5] Sinn H, Alp E E, Alatas A, Barraza J, Bortel G, Burkel E, Shu D, Sturhahn W, Sutter J P, Toellner T S and Zhao J 2001 *Proc. SRI-2000; Nucl. Instrum. Methods* A at press
[6] Baron A Q R, Tanaka Y, Miwa D, Ishikawa D, Mochizuki T, Takeshita K, Goto S, Matsushita T and Ishikawa T 2001 *Proc. SRI-2000; Nucl. Instrum. Methods* A at press
[7] Burkel E 2000 *Rep. Prog. Phys.* **63** 171
[8] Schülke W 1991 *Inelastic Scattering by Electronic Excitations (Handbook on Synchrotron Radiation vol 3)* ed G Brown and D E Moncton (Amsterdam: Elsevier Science)
[9] Chihara J 2000 *J. Phys.: Condens. Matter* **12** 231
[10] Platzman P M and Tzoar N 1973 *Phys. Rev.* B **7** 2450
[11] Alatas A 2001 Form factor studies in beryllium *PhD Thesis* Illinois Institute of Technology, IL, in preparation
[12] James R W 1963 *The Dynamical Theory of X-ray Diffraction in the Solid State* vol 15, ed F Seitz and D Turnbull (London: Academic)
[13] Sutter J P, Alp E E, Hu M Y, Lee P L, Sinn H, Sturhahn W, Toellner T S, Bortel G and Colella R 2001 *Phys. Rev.* B at press
[14] Shvydko Yu V, Gerdau E, Jäschke J, Leupold O, Lucht M and Rüter H D 1998 *Phys. Rev.* B **57** 4968
Shvydko Yu V, Gerdau E, Gerken M, Lerche M, Lucht M, Rüter H D, Wille H C, Alp E, Sinn H, Sutter J and Alatas A 2001 *Proc. SRI-2000; Nucl. Instrum. Methods* A at press
[15] Sinn H 1991 Röntgenstreuung mit hoher Energieauflösung an kollektiven Dichtmoden in flüssigem Lithium *Diploma Thesis* University of Munich
[16] Verbeni R *et al* 1996 *J. Synchrotron Radiat.* **3** 62
[17] Okada Y and Tokumaru Y 1984 *J. Appl. Phys.* **56** 314
[18] Toellner T S 2000 *Hyperfine Interact.* **125** 3
[19] Lovesey S W 1984 *Theory of Neutron Scattering from Condensed Matter* vol 1 (Oxford: Clarendon)
[20] Hansen J-P and McDonald I R 1986 *Theory of Simple Liquids* (London: Academic)